

# Aponeurosis Structure-Function Properties: Evidence of Heterogeneity and Implications for Muscle Function

Benjamin B. Wheatley<sup>1\*</sup>, Olivia L. Dyer<sup>2</sup>, Emily E. Tully<sup>1</sup>, & Mark A. Seeley<sup>2</sup>

<sup>1</sup>Department of Mechanical Engineering, Bucknell University, Lewisburg, PA

<sup>2</sup>Musculoskeletal Institute, Geisinger, Danville, PA

\*Corresponding Author:

[b.wheatley@bucknell.edu](mailto:b.wheatley@bucknell.edu)

Academic East 302

1 Dent Drive

Lewisburg, PA 17837

Keywords:

hyperelastic; skeletal muscle; finite element; materials testing; finite element modeling; microstructure; scanning electron microscopy

Abstract:

Aponeurosis is a sheath-like connective tissue that aids in force transmission from muscle to tendon and can be found throughout the musculoskeletal system. The key role of aponeurosis in muscle-tendon unit mechanics is clouded by a lack of understanding of aponeurosis structure-function properties. This work aimed to determine the heterogeneous material properties of porcine triceps brachii aponeurosis tissue with materials testing and evaluate heterogeneous aponeurosis microstructure with scanning electron microscopy. We found that aponeurosis may exhibit more microstructural collagen waviness in the insertion region (near the tendon) compared to the transition region (near the muscle midbelly) (1.20 versus 1.12,  $p=0.055$ ), which and a less stiff stress-strain response in the insertion versus transition regions ( $p<0.05$ ). We also showed that different assumptions of aponeurosis heterogeneity, specifically variations in elastic modulus with location can alter the stiffness (by more than 10x) and strain (by approximately 10% muscle fiber strain) of a finite element model of muscle and aponeurosis. Collectively, these results suggest that aponeurosis heterogeneity could be due to variations in tissue microstructure and that different approaches to modeling tissue heterogeneity alters the behavior of computational models of muscle-tendon units.

## 1. Introduction

Aponeurosis is a sheath-like connective tissue found in many muscle tendon units that aids in force transmission from soft, contractile muscle to stiff, passive tendon, and thus plays a crucial role in the mechanical function of the musculoskeletal system [1–3]. A considerable fraction of muscle fibers insert directly into aponeurosis, which transitions to tendon or attaches directly to bone or other soft tissue. Aponeurosis enables variability in muscle-tendon unit architecture, which manifests in different muscle-tendon unit properties such as higher forces or faster contraction velocities [4]. Additionally, aponeurosis geometry and material properties are closely related to muscle-tendon unit function, as changes to aponeurosis can affect muscle strain and muscle gearing [2,5–7]. It is generally observed that aponeurosis thickness is heterogeneous within and across muscle-tendon units, often thinning as the tissue transitions from tendon to muscle, and aponeurosis thickness is positively correlated to muscle size and force generating capacity [5,8–11]. Aponeurosis morphology also varies across muscles, species, and individuals, ranging from thin, exterior sheets to thicker interior structures.

Aponeurosis has traditionally been viewed as an extension of tendon, acting in series with muscle [12,13]. However, due to the complex architecture and function of muscle-tendon units, the assumption of series elasticity is likely to be incorrect, suggesting that the role of aponeurosis in force transmission is far more complex [2,14–16]. Specifically, aponeurosis apparent stiffness varies depending on active versus passive muscle forces and aponeurosis is subject to biaxial loading *in vivo*, both of which negate a simple series elasticity assumption with muscle [7,14,17–19]. It has also recently been suggested that aponeurosis could act as a type of pulley for connected muscle fibers, thus contradicting the age-old assumption that muscle pennation angle affects force output [20]. Thus, the exact role of force transmission from muscle fibers through aponeurosis to tendon remains unexplained by a unified model [21]. One reason for this lack of a unified model is a rather limited understanding of the specific structure-function mechanisms of aponeurosis tissue, which may help to explain this multi-axial behavior, tissue heterogeneity, and differences in aponeurosis function under active and passive conditions.

A major challenge in muscle-tendon unit mechanics research is the difficulty of evaluating material properties of muscle and aponeurosis *in vivo*. The geometry of a muscle-tendon unit makes direct aponeurosis force measurements a challenge that has not yet been overcome [19,21]. Thus, materials testing of excised tissue samples under carefully controlled experimental environments are the current gold standard for material property estimation, despite the fact that these approaches remove the tissue from the native mechanical environment. To the best of the authors' knowledge, there have been two previously published studies that have combined materials testing and structural imaging of aponeurosis, both of which qualitatively showed a collagen-rich structure with aligned, wavy fibers [22,23]. Previous materials characterization works of aponeurosis have shown properties common to biological soft tissues such as anisotropy, nonlinearity, viscoelasticity, and heterogeneity [10,22–24]. Specifically, aponeurosis is highly anisotropic with a longitudinal modulus between 50-750 MPa and a transverse modulus of 0.3-100 MPa, which is greater than the approximate modulus of muscle (~0.1 MPa) and comparable to that of tendon (~1000 MPa) [22–24]. Aponeurosis nonlinearity can be described by a nonlinear toe-region followed by a linear region, which suggests collagen waviness plays a key role in tissue stiffness [22]. One study of gastrocnemius and soleus samples from human cadavers found that a region of the anterior gastrocnemius lateralis aponeurosis exhibited an

elastic modulus of nearly twice that of a region of the anterior lateral soleus aponeurosis (324 MPa vs 164 MPa, respectively) [10]. There is also variability in species and specific muscle-tendon units used for aponeurosis materials testing studies, ranging from human gastrocnemius and soleus [10] to turkey gastrocnemius [22] and porcine triceps brachii [23].

Despite these numerous *in vitro* studies on aponeurosis mechanics, aponeurosis material properties have not been directly attributed to quantified microstructural measures. While our previous work [23] showed that collagen-rich aponeurosis [25] exhibits variability in collagen orientation, the specific structure-function mechanisms for aponeurosis heterogeneity remain unknown. It would be expected that aponeurosis and tendon exhibit similar structure function mechanisms, where measures such as collagen waviness and alignment influence tissue stiffness, specifically stiffer tissue exhibits highly aligned, straight collagen fibers [26–28]. Experimental techniques such as tissue fixing and scanning electron microscopy have been previously used for microstructural analysis, and can be used under undeformed and deformed conditions to study changes in tissue microstructure with stretch [23,29].

Parsing the role of aponeurosis in locomotion is a challenge due to the difficulties studying *in vivo* function of muscle tendon units, the wide variability of muscle-tendon unit properties, and the complex three-dimensional nature of muscle contraction [3]. However, computational models of muscle-tendon units can be used to complement and enhance experimental studies and can provide critical insight into musculoskeletal tissue function not easily obtained from experimentation. For example, studying the effects of perturbations in tissue properties such as stiffness on muscle-tendon unit function is considerably more straightforward *in silico* versus *in vivo*. Previous modeling work has shown that aponeurosis geometry significantly alters muscle stretch distributions [30], aponeurosis stiffness alters muscle force production [31], and muscle architecture affects aponeurosis stretch [32]. However, it is not known how the heterogeneity of aponeurosis may affect muscle-tendon unit function, and the previously detailed gap in aponeurosis structure-function mechanisms hampers the accuracy of computational modeling where material properties are not known.

Thus, two major questions remain in aponeurosis mechanics. First, what are the contributors to the heterogeneity of aponeurosis material properties? Second, how does the heterogeneity of aponeurosis material properties affect muscle-tendon unit function? In an effort towards answering these questions, we have chosen to employ tissue-level materials testing to characterize the heterogeneity of porcine triceps brachii aponeurosis material properties, scanning electron microscopy to characterize the heterogeneity of aponeurosis microstructure, and finite element modeling to study the effects of aponeurosis heterogeneity on muscle-tendon unit function. We hypothesized that a) aponeurosis modulus would be higher near the tendon (where transmitted forces could be higher), b) aponeurosis collagen microstructure would be less wavy near the tendon (hence straighter fibers are associated with stiffer tissue behavior), and c) that the stiffness of a finite element model of muscle and aponeurosis would be altered by assumptions of aponeurosis heterogeneity.

## **2. Methods**

### **2.1 Sample Preparation**

Porcine shoulder tissue was obtained from a local abattoir and aponeurosis tissue was dissected from the triceps brachii muscle using standard dissection techniques [22,23]. No live animal handling was performed by any members of the research team. All testing was completed or tissue fixation was initiated within two days of tissue acquisition. Throughout dissection and materials testing, samples were kept moist by applying a phosphate buffered saline solution [33]. Once the sheet of aponeurosis tissue was dissected away from the muscle (with only a small amount of residual muscle remaining on each sample), then 60mm x10mm tissue samples were extracted from the midsection of each isolated aponeurosis section using a scalpel, ensuring that the samples include the transition from thick (the insertion region) to thin (the transition region) aponeurosis tissue (Figure 1A). All samples were oriented in the longitudinal or fiber direction. Each dissected tissue sample was marked in 5mm increments along the tissue with a permanent marker. Using a standard dissection microscope, four evenly spaced thickness measurements of aponeurosis tissue only (ignoring any small amount of residual muscle tissue) were taken between each 5 mm marking in the middle 40 mm of each sample, for a total of 32 total thickness measurements per sample [23].

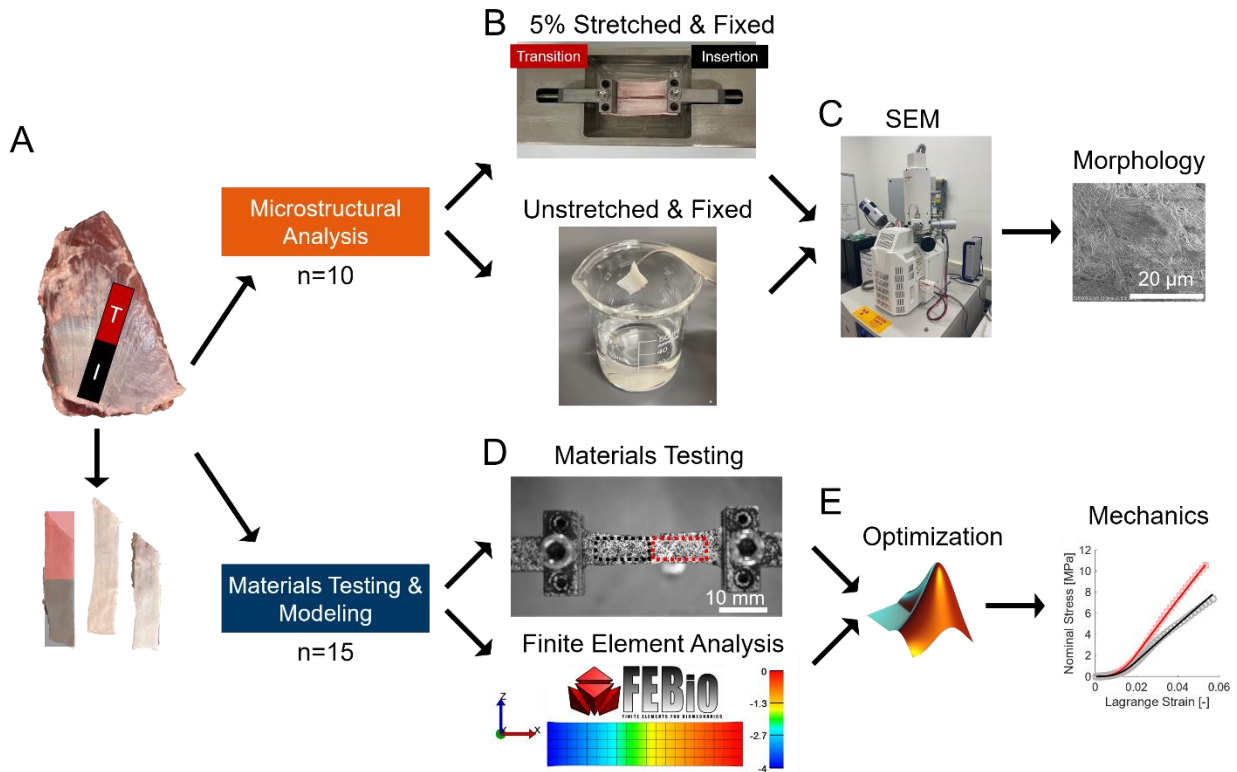


Figure 1. Overview of structure-function characterization methods. A) Aponeurosis tissue showing insertion (I – near tendon) and transition (T – near muscle midbelly) regions. B) Structural analysis was performed on stretched and unstretched (n=10 each) fixed samples with a custom tissue stretcher. C) Scanning electron microscopy was used to evaluate morphological characteristics of tissue microstructure. D) Uniaxial tensile testing (n=15) was performed with 2D strain tracking through digital image correlation (transition region – red dotted box, and insertion region – black dotted box) along with finite element analysis of the experiment. E) Nonlinear optimization in MATLAB was used to fit model stress-strain curves with experimental stress-strain curves to extract material parameter values.

## 2.4 Microstructure Characterization

For microstructural analysis, dissected, unstretched aponeurosis samples (n=10) were immediately placed in a 1:20 volume ratio of 10% formaldehyde at 4°C for 24 hours (Figure 1B). Samples were subject to a series of graded ethanol soakings that included 15min in 30% ethanol, 15min in 50% ethanol, 15min in 70% ethanol, 15min in 90% ethanol, 15min in 100% ethanol, and finally 30min in 100% ethanol followed by soaking in a 1:2 solution of Hexamethyldisilazane (HMDS) to ethanol for 20min and a 20min soaking in 2:1 solution of HMDS to ethanol. Samples were then fully dehydrated in two 20min soakings in 100% HMDS. The final HMDS was poured off to just cover the top of the samples and they were left in the fume hood to evaporate overnight [34,35]. For stretched tissue, dissected aponeurosis samples (n=10) were immediately placed in a custom tissue stretcher with serrated grips and stretched to five percent of initial manually pre-tensioned length using digital calipers to measure grip distance (Figure 1B), based on materials testing data collected in this work that suggests at 5% strain, aponeurosis is within the linear region of the stress-strain curve and is sub-failure. The same fixative approach described above was used.

After full dehydration, a Hitachi SU5000 Field Emission Gun Microscope was used for scanning electron microscopy (Figure 1C). First, samples were imaged under low vacuum pressure to observe low magnification (50x-100x) structural features [36]. Following low magnification imaging, samples were sputter coated with gold and placed back into the SEM for imaging under high vacuum pressure at high magnification (1,000x-3,500x) (Figure 1C). Images were taken at 50, 100, 1,000, and 3,500 magnifications along each aponeurosis sample. Additional images were taken at 10,000 and 50,000 magnifications for some of the unstretched samples to help characterize the general microstructure of the tissue. Scanning electron microscope images were loaded into FIJI/ImageJ to evaluate collagen fiber waviness using the *NeuronJ* plugin [37]. For each sample, 2-3 waviness measurements were made at 3 locations, totaling 6-9 measurements per sample. Waviness of the stretched and unstretched aponeurosis was quantified as the ratio of the true length of the collagen fiber to the tangent of that same collagen fiber [29].

## 2.3 Materials Testing

Uniaxial tensile testing was completed on a custom planar biaxial material testing system (ADMET, Inc., Norwood, MA) on n=15 samples. All samples were clamped with serrated grips with a 40 mm gage length (10 mm of aponeurosis in each grip) and the strain rate for the tensile test was set to 0.05% sec<sup>-1</sup> elongation after a 0.1 N pre-load [23,38,39]. Charcoal powder was lightly dusted onto the sample through a sifter for digital image correlation (DIC) (Figure 1B) with an image capture rate of 0.5 seconds. Grip slippage was addressed with interlocking pyramid grips and digital image correlation. Digital image correlation was performed using commercial software to measure the heterogeneous Lagrange strain of each sample (Vic2D, Correlated Solutions, Inc.) [23,39]. One midsection region of interest was manually selected to avoid edge effects near the grips, which was then subdivided into two equal areas in post processing (Figure 1D). Force-displacement curves were manually condensed to only the toe-region and linear elastic regions (all damage and failure data was removed based on visual inspection) [39,40]. Using the uniaxial force data, inhomogeneous 2D DIC data, and thickness measurements, the average nominal (engineering) stress and Lagrange strain values were determined for two sections of each sample, one considered the ‘transition region’, where the

aponeurosis tissue connects to muscle fibers and is thinner, and the other considered the ‘insertion region’, where the aponeurosis tissue connects to the tendon tissue and is thicker.

## 2.4 Finite Element Modeling

Two different finite element model geometries were implemented in this study – one model of isolated aponeurosis tensile testing samples and one model of idealized muscle and aponeurosis tissue. All finite element modeling was performed in FEBio [41]. First, a simple hexahedral shaped geometry to mimic experimental tensile tests was developed with a 40 mm nominal length, 10 mm nominal width, and mean thickness values at each of the 32 measurement locations along the aponeurosis from all samples (Figure 2A, 100 first-order hexahedral elements). To generate this geometry, a 3D model was developed in SolidWorks that connected the 32 points with a spline, which was then exported for hexahedral meshing. This mesh density was chosen based on prior modeling of similar simple geometries of biological soft tissue [42]. To mimic experimental materials testing, one end of the model was pinned while the other end was displaced 4 mm (10% nominal strain). Reaction force and mean Lagrange strain of each region (insertion and transition) was recorded and converted to stress-strain curves similar to experimental procedures. All model data above experimentally observed strain (~6% Lagrange strain) were then discarded.

A transversely isotropic, hyperelastic constitutive model was used for aponeurosis tissue that combined an isotropic, uncoupled first-order Ogden model and an anisotropic, fiber-reinforcing component (Equation 1). The first-order Ogden model (Equation 2) uses material parameters  $c$  and  $m$  and is a function of the deviatoric (volume-constant) principal stretches  $\tilde{\lambda}_{1-3}$  and the volumetric component (Equation 3) incorporates a bulk modulus  $k$  and is a function of the volume ratio  $J$ . For this study,  $c = 0.2$  MPa,  $m = 40$ , and  $k = 1$  GPa values were used based on our prior work characterizing anisotropic material properties of aponeurosis tissue [23]. The anisotropic, tension-only reinforcing fiber contribution (Equation 4) is a function of deviatoric fiber stretch  $\tilde{\lambda}_4$  and includes a power law toe-region and a linear region. Here the material parameters are the transition stretch  $\lambda_0$  (the stretch at which the material transitions from the toe-region to the linear region), toe-region nonlinearity  $\beta$ , and the linear region modulus  $E(X)$ . It should be noted the parameters  $\xi$  and  $B$  are calculated to maintain continuity of the tangent modulus function for model stability and are thus not inputs into the constitutive formulation.

$$\Psi(\tilde{\lambda}_1, \tilde{\lambda}_2, \tilde{\lambda}_3, J, \tilde{\lambda}_4) = \Psi^{iso}(\tilde{\lambda}_1, \tilde{\lambda}_2, \tilde{\lambda}_3) + \Psi^{vol}(J) + \Psi^{aniso}(\tilde{\lambda}_4) \quad (1)$$

$$\Psi^{iso}(\tilde{\lambda}_1, \tilde{\lambda}_2, \tilde{\lambda}_3) = \frac{c}{m^2} (\tilde{\lambda}_1^m + \tilde{\lambda}_2^m + \tilde{\lambda}_3^m - 3) \quad (2)$$

$$\Psi^{vol}(J) = \frac{1}{2} k \ln(J)^2 \quad (3)$$

$$\Psi^{aniso}(\tilde{\lambda}_4) = \begin{cases} 0, & \tilde{\lambda}_4 < 1 \\ \frac{\xi}{\beta} (\tilde{\lambda}_4^2 - 1), & 1 \leq \tilde{\lambda}_4 \leq \lambda_0 \\ B(\tilde{\lambda}_4^2 - \lambda_0^2) - E(X)(\tilde{\lambda}_4 - \lambda_0) + \frac{\xi}{\beta} (\lambda_0^2 - 1), & \lambda_0 < \tilde{\lambda}_4 \end{cases} \quad (4)$$

To investigate the effect of aponeurosis location on material properties using finite element analysis, the linear region elastic modulus was defined as a function of initial reference coordinate system location along the  $X$  axis. For this study, we used three different functions to study a range of possible aponeurosis behavior – 1) a constant modulus (Equation 5, where  $a_1$  is the elastic modulus MPa and  $b_1 = 0$ ), 2) a linearly varying modulus (Equation 5, where  $a_1$  and  $b_1$  are material parameters in MPa), and 3) a log-normal function (Equation 6, where  $a_1$  and  $b_1$  are material parameters in MPa and  $\mu$  mm and unitless  $\sigma$  are chosen, fixed values).

$$E(X) = a_1 + b_1X \quad (5)$$

$$E(X) = a_2 + b_2 \operatorname{erfc} \left[ -\frac{\ln\left(\frac{X}{\mu}\right)}{\sigma\sqrt{2}} \right] \quad (6)$$

An inverse finite element modeling optimization approach was employed to fit finite element model stress-strain curves to experimental stress-strain curves and extract finite element model constitutive parameters (Figure 1E). This approach has been employed in myriad studies to generate material properties of biological soft tissues where an analytical approach is not feasible [39,43–45], including our previous work characterizing biaxial tensile properties of aponeurosis [23]. Briefly, the nonlinear optimization function *lsqnonlin* in MATLAB (The Mathworks, Inc.) was used to reduce the residuals between mean experimental and model stress-strain curves (both the transition region and insertion region) by varying the following four constitutive parameters: transition stretch  $\lambda_0$ , toe-region nonlinearity  $\beta$ , and linear region modulus parameters  $a_1/a_2$ , and  $b_1/b_2$ . A range of different initial guesses were used to ensure global convergence. The log normal formulation (Equation 6) was fit to both the mean stress-strain curves for the transition and insertion regions (model denoted as “LNM” for log normal mean) as well as a set of stress-strain curves generated by the mean and standard errors of experimental data (model denoted as “LNS” for log normal standard error) to explore extreme ranges of the data set. Thus, this optimization produced four sets of aponeurosis parameters with variable heterogeneity for the same constitutive model – constant, linear, LNM, and LNS (Figure 2C).

The second finite element model used in this study was developed based on the 2D geometry of a slice of a full skeletal muscle (Figure 2B, 560 second-order hexahedral elements). Mesh convergence was achieved based on comparisons to a model of 954 elements, which yielded less than a 1% difference in all outputs reported in this study. Similar geometries have been used in finite element analysis of skeletal muscle and muscle-tendon unit function to study the effects of various assumptions on muscle and aponeurosis behavior [32,46]. This model incorporated two separate aponeuroses and unipennate skeletal muscle. The overall model length was 100 mm (each aponeurosis of length 80 mm), muscle pennation angle was 40° (thus muscle fiber length was 24.4 mm), model thickness was 2 mm, and aponeurosis thickness linearly decreased from 1.25 mm to 0.25 mm from the insertion to the transition regions, which approximately matches our experimentally measured thickness values.

The validated muscle constitutive model used in this study is detailed in Wheatley et al., 2018. Briefly, muscle is modeled as a transversely isotropic material with a set of passive reinforcing 3D fibers (representing the stiffness of the extracellular matrix and muscle fibers) and a set of

active 1D fibers (representing the contractile components of muscle tissue). The model was pinned at one end and subject to two sets of boundary conditions: one passive condition where the other end was displaced in the X-direction 20 mm (simulating 20% passive strain of the whole system) and one active condition where the other end was fixed in the X-direction and the muscle material generated 0.5 MPa of active stress (simulating an isometric contraction of 30 N/cm<sup>2</sup>) [48–50]. All four sets of optimized aponeurosis constitutive parameters, as detailed above, were employed in otherwise identical simulations – constant, linear, LNM, and LNS (Figure 2C). Full model aponeurosis fiber strain, muscle fiber strain, and reaction force were recorded from each simulation for comparisons.

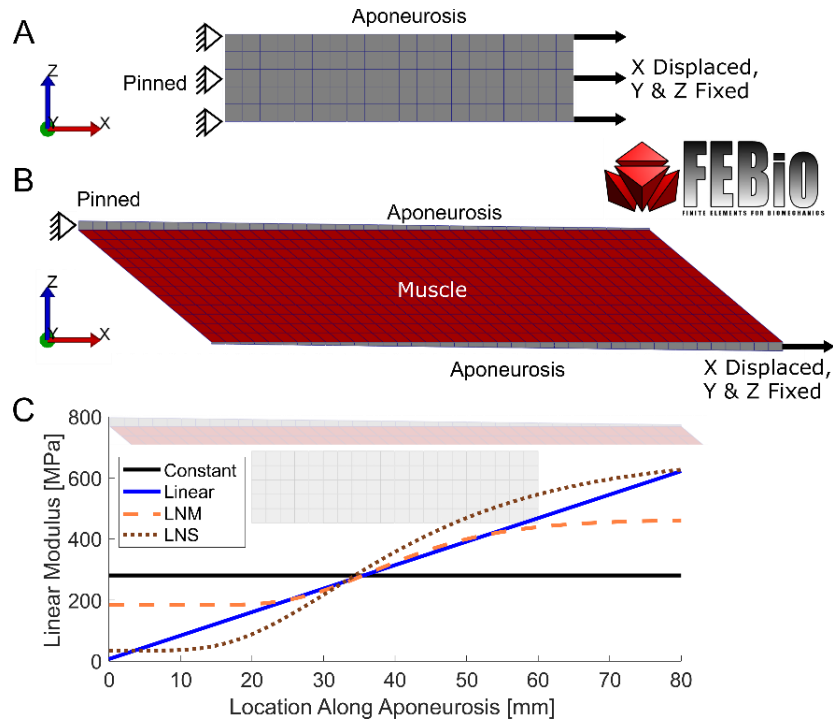


Figure 2. Finite element modeling approaches. A) Isolated aponeurosis model mesh, geometry (40 mm length in X, 10 mm width in Z, and variable thickness in Y) and boundary conditions (left face pinned, right face fixed in Y and Z and displaced in X). B) Muscle slice model mesh, geometry, and boundary conditions (top left point pinned, bottom right point displaced in X-direction with no other boundary conditions, and front face fixed in the Y-direction). C)

Variations in aponeurosis linear modulus as a function of location for various models. The isolated aponeurosis model and muscle slice models are aligned in the background such that the linear modulus values in the graph correspond to the specific model locations.

## 2.5 Statistics

A linear regression was performed on all thickness data to evaluate any relationship between aponeurosis location and tissue thickness (significance set at  $p < 0.05$ ). For microstructural waviness comparisons between regions and the unstretched/stretched groups, unpaired, two-way t-tests were used with significance set at  $p < 0.05$ . For stress-strain comparisons between regions, tangent moduli for each region were calculated by a linear fit to a moving subset of 100 data points throughout the stress-strain curves and stress:strain ratios of each region were determined at each time point by dividing nominal stress by Lagrange strain. Paired t-tests (significance set

at  $p < 0.05$ ) were performed on the tangent moduli and stress:strain ratios at each time point using statistical parametric mapping to determine any statistically significant differences in the stress-strain curves between the transition and insertion regions [51]. Inverse finite element optimization fits were quantified by calculating the normalized root mean square error, which is a measure of overall fit error reported as a percentage [44]. All error bars shown in results figures are standard error of the mean.

### 3. Results

Aponeurosis increased in thickness from the transition region (near muscle midbelly) to the insertion region (where muscle and aponeurosis connects to tendon) (Figure 3). The mean thickness of the first transition region (least thick) was 0.56 mm and the mean thickness of the final insertion region (most thick) was 0.87 mm (Figure 3A). Linear regression results showed a wide spread in thickness values across samples and a positive correlation between thickness and location ( $R^2=0.50$ ,  $p < 0.001$ , Figure 3B).

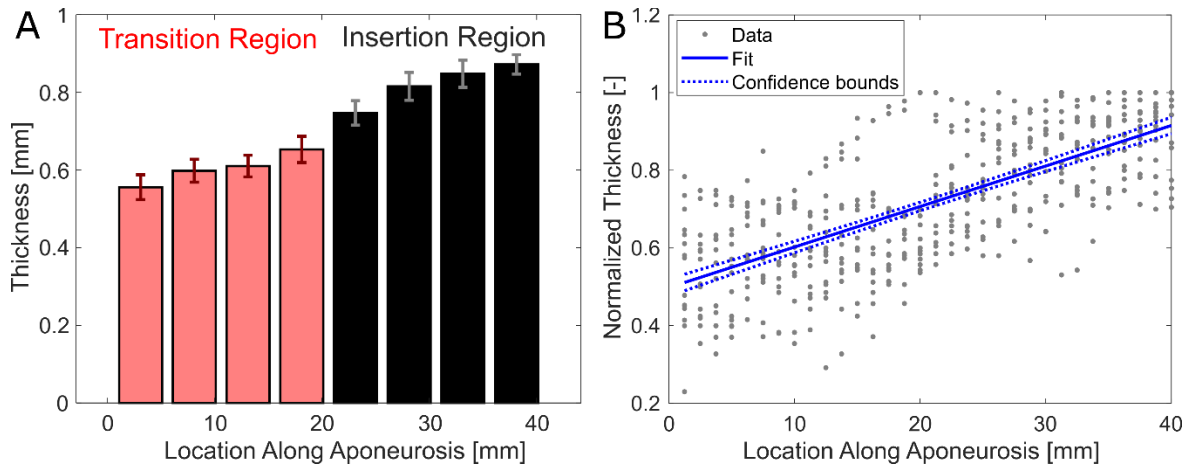


Figure 3. Aponeurosis thickness results. A) Mean thickness values (with standard error bars) as a function of aponeurosis length within the materials testing region of interest for transition and insertion regions. B) Linear regression results ( $R^2=0.18$ ,  $p < 0.001$ ) showed an increase in aponeurosis thickness from the transition to the insertion region.

Scanning electron microscopy showed that aponeurosis tissue exhibits a hierarchical structure, similar to that of tendon or ligament, with collagen-rich fascicles (75 $\mu\text{m}$  to 200 $\mu\text{m}$  diameter), fibers (50 $\mu\text{m}$  to 20 $\mu\text{m}$  diameter), and fibrils (10-300nm) (Figure 4). Waviness and alignment in the collagen fibers was observed at lower magnifications (Figure 4A), while at higher magnifications aponeurosis exhibits a sheet-like structure with less organization (Figure 4B).

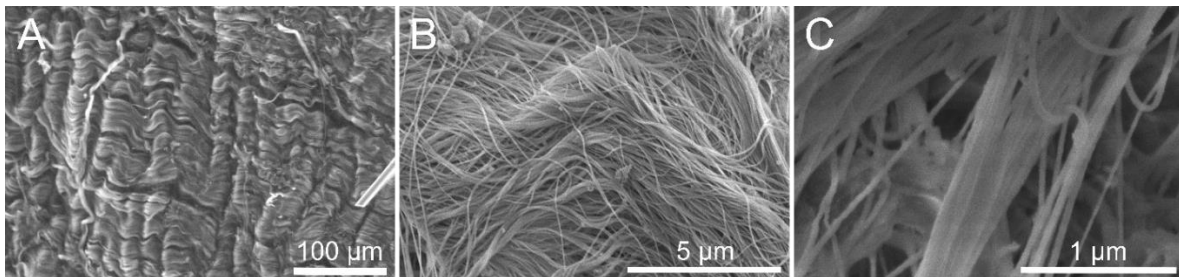


Figure 4. SEM images of unstretched porcine triceps brachii at (A) 300x magnification, (B) 10,000x magnification, and (C) 50,000x magnification. Collagen crimp and waviness in the fibers is highly observed at lower magnifications while the sheet like structure is observed in the higher magnifications.

Unstretched tissue had an average waviness value of 1.17, with values ranging from 1.00 to 1.45 (Figure 5A-B). Waviness values from the insertion region were found to be  $1.20 \pm 0.24$  (mean  $\pm$  standard deviation) and  $1.12 \pm 0.14$  for the transition region, although statistically these differences were trending but not significant at  $\alpha < 0.05$  ( $p = 0.055$ , Table 1). In contrast, the stretched tissue had an average waviness value of 1.05, which was statistically significant compared to unstretched tissue ( $p < 0.001$ ) (Figure 5C-D). Waviness values from the insertion and transition regions in the stretched tissue were not different ( $p = 0.45$ ).

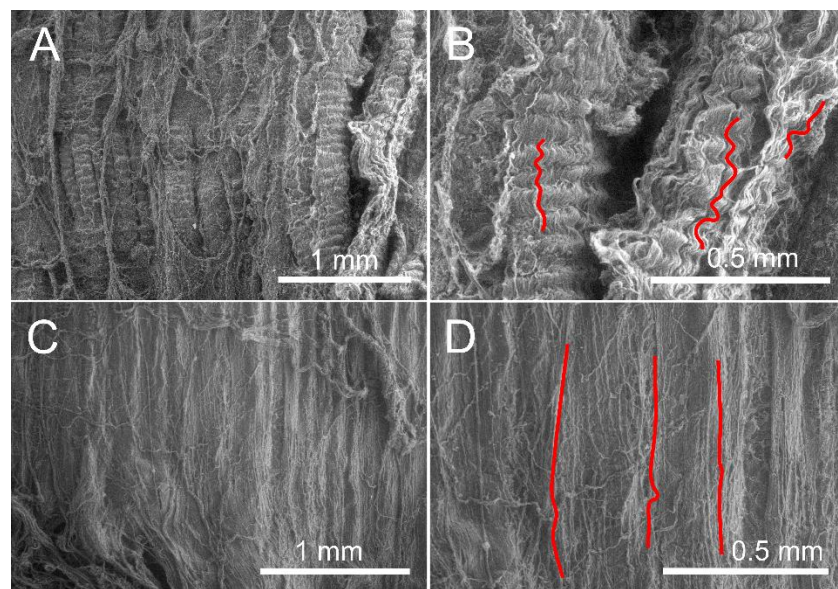


Figure 5. (A/B) SEM images of unstretched porcine triceps brachii at (A) 40x magnification and (B) 100x magnification. Collagen crimp is highly observed in the 40x and 100x magnification and the average waviness values of the unstretched aponeurosis tissue was  $1.174 \pm 0.211$ . (C/D) SEM images of five percent stretched porcine triceps brachii at (C) 40x magnification and (D) 100x magnification. The waviness of collagen fibers is drastically reduced once stretched five percent.

Table 1. Waviness values of the unstretched and stretched tissue including combined and by region (mean  $\pm$  standard deviation). Comparing the combined waviness values of the unstretched and stretched tissue shows that there is a statistically significant difference in the waviness values. There was not a statistically significant difference comparing the insertion and transition regions within the unstretched and stretched tissue respectively, while there is a statistically significant difference when comparing the insertion and transition region across the two different groups.

	Unstretched Tissue	Stretched Tissue	p-value
<b>Combined</b>	$1.17 \pm 0.21$	$1.05 \pm 0.06$	$<0.001$
<b>Insertion Region</b>	$1.20 \pm 0.24$	$1.05 \pm 0.05$	$<0.001$

<b>Transition Region</b>	$1.12 \pm 0.14$	$1.05 \pm 0.08$	0.0054
<b>p-value</b>	0.055	0.45	

The stress-strain curves for both regions exhibited a nonlinear toe region and linear region (Figure 6A). The transition region (thinner, towards the muscle midbelly) exhibited a higher stress response and stiffer behavior, as characterized by the statistical parametric mapping paired t-tests. Specifically, the statistically significant differences were observed in tangent modulus throughout the toe-region and early linear region (Figure 6A, region where  $p < 0.05$  denoted by solid blue line) and stress:strain ratio throughout much of the stress-strain curve (Figure 6A, region where  $p < 0.05$  denoted by dashed blue line).

Fits to experimental data from the inverse finite element optimization (Figure 6B) showed the constant modulus approach (solid black curve) failed to capture the stress-strain response of the two regions (normalized root mean square error 32%). However, the linear and LNM approaches provided strong fits to the mean transition and insertion stress-strain data (dashed red and black curves, normalized root mean square errors of 6.6% for the linear model, and 6.1% for the LNM model). It should be noted that the linear varying modulus and LNM varying modulus fits were nearly indistinguishable visually, and thus the linear varying modulus fit is only shown. Finally, the LNS model (Figure 6B, dotted red and black curves) provided a set of parameters for an exaggerated range in stress-strain behavior between regions (normalized root mean square error of 58%). Optimized parameters (Table 2) showed a wide range of optimized modulus values and very little variation in toe-region nonlinearity ( $\beta \approx 4.25$ ) and transition stretch ( $\lambda_0 \approx 1.017$ ) across modeling approaches.

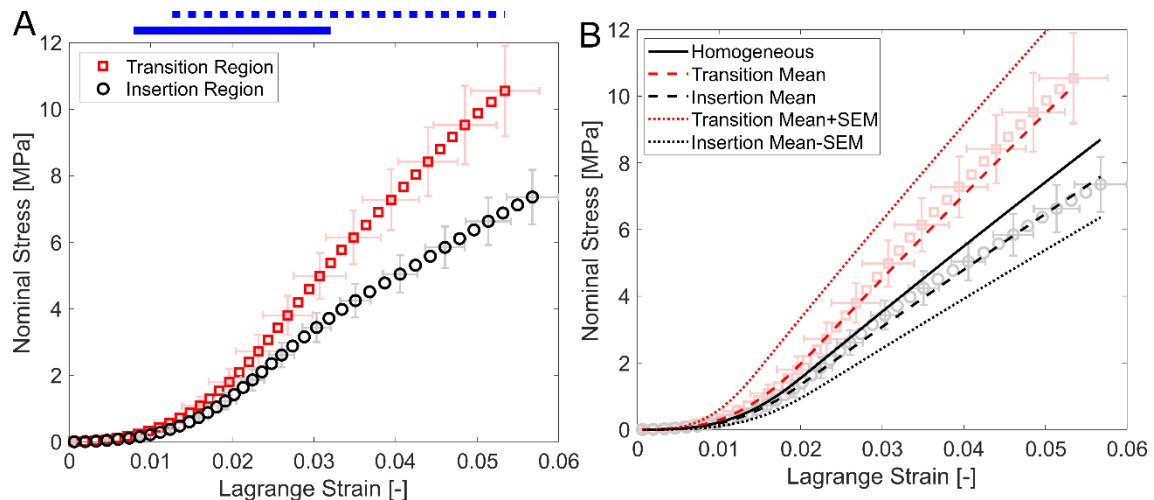


Figure 6. A) Mean stress strain data (with standard error bars) graphed for the insertion (black circles) and transition (red squares) regions. The blue solid bar above the graph denotes the region of the stress-strain curve where the differences in tangent moduli between the two data sets are statistically significant ( $p < 0.05$ ), and the dashed blue bar above the graph denotes the region of the stress-strain curve where the differences in stress:strain ratio between the two data sets are statistically significant ( $p < 0.05$ ). B) Optimized finite element model fits to experimental data for various modulus modeling approaches. Optimizations include a homogeneous modulus fit (solid curve), varying moduli fits (linear and LNM – dashed curves) to the mean transition and insertion stress-strain data, and LNS (dotted curves) to the mean  $\pm$  standard error data.

Note that the linear and LNM fits to the mean data were virtually indistinguishable visually, thus only the linear fit is shown here.

Table 2. Optimized aponeurosis material parameters for all four approaches to modeling aponeurosis heterogeneity. The log normal optimizations each used a value for  $\mu = 40$  mm and the LNM and LNS optimizations used  $\sigma$  values of 0.3 and 0.5, respectively.

Parameter	Constant	Linear	LNM (Log Normal Mean)	LNS (Log Normal Mean/SEM)
$a_1$ or $a_2$ [MPa]	281	161	185	44.7
$b_1$ or $b_2$ [MPa]	0	7.69	140	499
$\beta$ [-]	4.25	4.25	4.26	4.64
$\lambda_0$ [-]	1.0169	1.0169	1.0170	1.0168

Muscle slice finite element modeling results showed that the constant and LNM models exhibited similar characteristics (aponeurosis and muscle fiber strains and reaction forces), while the linear and LNS models exhibited similar characteristics (Figure 7). Specifically, the mean aponeurosis strain was nearly double in the linear model compared to the constant model under both passive stretch (0.12 versus 0.070) and activation (0.056 versus 0.032) (Figure 7A). Muscle fiber strain showed less variability, but mean values ranged from 0.31 to 0.45 under passive stretch and -0.15 to -0.24 under active contraction (Figure 7B). Reaction force curves showed a wide range of behavior, as the constant and LNM models exhibited highly nonlinear, stiff passive behavior and a higher reaction force under active conditions when compared to the linear and LNS models (Figure 7C). At a passive stretch of 0.2 whole muscle strain, the constant model reaction force was 45.9 N versus 3.80 N for the linear model. These differences were smaller for active contraction conditions, as the constant model reaction force was 17.1 N versus 3.63 N for the linear model.

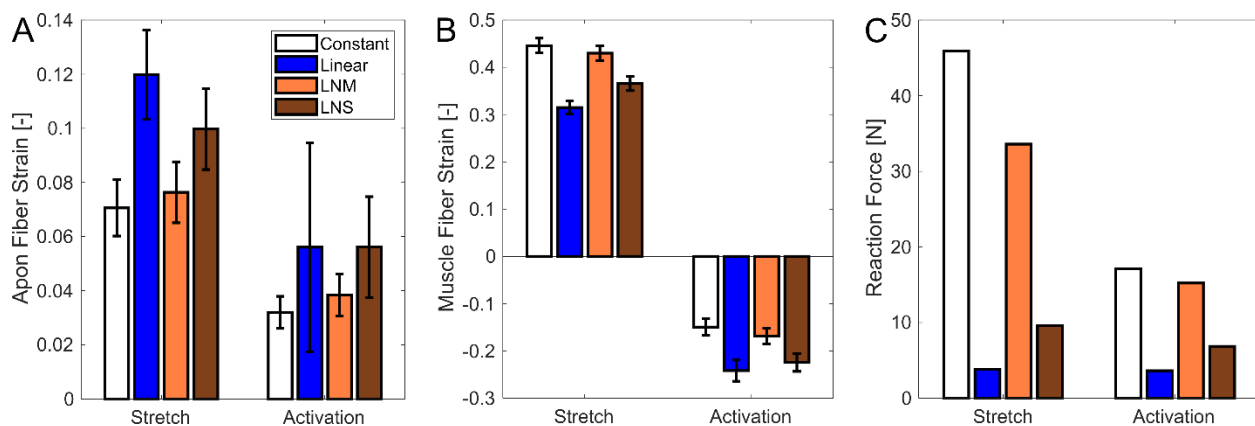


Figure 7. Muscle slice finite element modeling results. A) Mean (with standard deviation bars) aponeurosis fiber strain during passive stretch and activation. B) Mean (with standard deviation bars) muscle fiber strain during passive stretch and activation. C) Whole model reaction force (measured at displacement node) for both passive stretch and activation.

#### 4. Discussion

This work characterizes heterogeneous structure-function properties of aponeurosis tissue and uses finite element analysis to study the implications of aponeurosis heterogeneity on muscle-tendon unit function. We present here, for the first time, a study that measured the heterogeneous collagen microstructure of aponeurosis tissue and how that microstructure is altered by stretch. We also performed uniaxial tensile testing, 2D digital image correlation, and inverse finite element analysis to determine material parameters of aponeurosis tissue given various assumptions of elastic modulus heterogeneity. Finally, we studied how these assumptions affect skeletal muscle modeling results with a finite element model of a muscle-aponeurosis structure. Our findings can be used to better understand how aponeurosis transmits force *in vivo* and to inform future models of the musculoskeletal system.

This work is not without limitations. First, we subdivided aponeurosis samples into only two regions (transition and insertion) based on dissection variability and digital image correlation accuracy and did not measure variations in thickness across the width of each sample (only sample length). Future work to investigate heterogeneity with greater spatial resolution would benefit the field. We have also chosen to neglect viscoelastic effects and test samples at quasi-static strain rates for simplicity. Additionally, the use of scanning electron microscopy for microstructural analysis provides surface imaging only. Future work to investigate through-thickness aponeurosis structure and imaging of the muscle-aponeurosis junction would be a major contribution to our understanding of aponeurosis structure. Our optimized material parameter  $\lambda_0 \approx 1.017$  also did not agree with our experimentally observed initial collagen waviness values between 1.12-1.20, which may be due to tissue shrinkage from fixing or more intricate deformation mechanisms than those captured from a tissue-level constitutive model. However, we expect the effect of tissue shrinkage to be minimal based on previously published work [52–54]. While the modeling completed in this work uses a particular constitutive model for skeletal muscle tissue based on our prior work [47,55], other formulations in literature [46,56–60] could possibly lead to differences in predicted model strains and stiffnesses. We also used thin, superficial, sheet-like porcine triceps brachii aponeurosis tissue, and while one might expect aponeuroses of similar structure to exhibit similar mechanical characteristics, it is not known exactly how the structure-function properties of human and porcine aponeurosis differ or how thin, superficial, sheet-like aponeurosis differs from thicker internal aponeurosis.

Finally, one important limitation of this work is that materials testing of *in vitro* aponeurosis samples removes aponeurosis from the *in vivo* environment, where muscle fibers insert into aponeurosis along the length of the tissue. As discussed in the introduction, direct force measurements in aponeurosis *in vivo* or *in situ* remain elusive in muscle physiology and mechanics research, which is the reason for the materials testing methods employed here [21]. Grip clamping each end of the tissue and applying a tensile load does not capture the native application of force from muscle fibers to aponeurosis tissue, which causes heterogeneous strain, biaxial loading, and differences in aponeurosis strain under active and passive conditions [14,19,61,62]. Nonetheless, our findings of structure-function mechanisms in aponeurosis tissue can be used to inform future work and are relevant for interpreting aponeurosis behavior under tensile conditions, which are common but not exclusive for aponeurosis *in vivo*.

Scanning electron microscopy confirmed the hierarchical structure of aponeurosis tissue from collagen fibrils to fibers and finally bundles, which mimics that of tendon and ligament [63,64],

but with a higher order sheet-like structure in place of a cylindrical structure (Figure 4). Azizi et al [22] imaged higher order aponeurosis structures, which showed aponeurosis fibers align with the orientation of tendon, and in our prior work [23] we showed that collagen microstructure orientation ranged within a single sample, suggesting aponeurosis exhibited heterogeneous structure. When paired with findings that aponeurosis is predominantly type I collagen [25], it is likely that collagen dominates the mechanical behavior of aponeurosis tissue.

Image analysis of scanning electron microscopy showed a collagen fiber waviness ratio in the insertion region of  $1.20 \pm 0.24$  (standard deviation) compared to the transition region value of  $1.12 \pm 0.14$  (standard deviation), which was trending towards statistical significance but not significant at  $\alpha=0.05$  ( $p=0.055$ , Figure 5 and Table 1). Nonetheless, waviness values of 1.20 and 1.12 between regions could certainly result in physiological differences, and may be statistically significant with a greater sample size. More waviness in the insertion region contradicts one of our prior hypotheses. With limited prior microstructural imaging of aponeurosis tissue, comparing these values to previously published work is a challenge, however mean waviness values of 1.17 compare favorably to similar measures of collagen waviness in muscle extracellular matrix [29,65]. We also observed a clear decrease in waviness from 1.17 down to 1.05 with only 5% stretch, suggesting that aponeurosis is experiencing heterogeneous stretch when loaded. These decreases in waviness agree with similar uncrimping observed in tendon [26,66]. These observations suggest that while muscle, aponeurosis, and tendon exhibit considerable differences in macrostructure and function, there may be similarities across tissues in collagen microstructure.

We also observed differences in stress-strain behavior between the two aponeurosis regions with tensile testing and digital image correlation. Specifically, the transition region exhibited more stiff behavior than the insertion region as characterized by both tangent modulus and stress:strain ratio (Figure 6), which also contradicts one of our prior hypotheses. In contrast to our findings, Zuurbier et al found greater strain in the transition region of aponeurosis with an *in situ* whole muscle-tendon unit study [19]. However, this disagreement could be due to differences in experimental protocols (whole muscle-tendon unit versus sectioned sample), specifically that *in situ* aponeurosis is not likely to experience a constant force across its length as compared to *in vitro* materials testing. Also, it should be noted that the stress-strain curves for each region reported in this work incorporate the surface strain and sample thickness for each region, while in Zuurbier et al only the surface displacement is reported. More collagen waviness in the insertion region would explain some of the differences in stress-strain behavior, especially in the toe-region of the stress-strain curve (Figure 6 solid blue line, which denotes statistical significance between tangent moduli at  $p<0.05$ ). Theoretically, differences in collagen waviness should primarily influence toe region length, which was not observed in our experimental data, suggesting more work is needed to predict aponeurosis stress-strain behavior with a microstructural model. Despite these challenges, we suggest, for the first time, that heterogeneous properties of aponeurosis tissue may be due to microstructural differences, specifically collagen waviness.

Our inverse finite element model optimization fits to experimental data (Figure 6B) show that a constant modulus is not capable of capturing the heterogeneous stress-strain behavior of aponeurosis tissue (32% normalized root mean square error), while our linearly varying and

LNM varying modulus models showed strong fits (~6% normalized root mean square error). Our optimized material properties, specifically modulus values that range from ~50-500 MPa, agree with previously published moduli values of aponeurosis tissue [10,22]. Prior work has shown that longitudinal aponeurosis fails approximately between 5-10% strain, thus our model fitting procedure appropriately characterizes the range of elastic tensile deformation of aponeurosis tissue [22,23]. Curiously, experimental heterogeneity was captured by variations in the modulus of our constitutive model, and not in the transition stretch or toe region nonlinearity (Table 2). Again, these differences between tissue structure-function mechanisms and our optimized model may be due to complex interactions at the microstructural level, which cannot be captured by our tissue-level model. Further work is needed in this area to explore this disconnect.

Our muscle slice modeling results show that differences in aponeurosis heterogeneity alter aponeurosis and muscle mechanics in a finite element model of a muscle-aponeurosis structure (Figure 7). Our model predicted a range of mean aponeurosis strain from 0.032 to 0.12, which agrees with experimental findings of maximum first principal aponeurosis strain between 0.075 and 0.25, even in maximal conditions [7,14,17,67]. We observed a nearly twofold increase in simulated mean aponeurosis fiber strain when transitioning from the constant modulus model (281 MPa) to the linear modulus model (increases of 615 MPa along aponeurosis length) (Figures 2 and 7). Our overall predicted mean muscle fiber strain (~0.2 shortening in isometric contraction and ~0.35 in passive elongation) agrees with experimental and computational studies that suggest muscle fibers can shorten as much as 0.3 strain (but typically 0.1-0.2) during isometric contractions [68,69] and withstand elongations up to 100% [30,70,71]. Mean muscle fiber strain differed between the constant and linear models by 0.14 strain under passive stretch and 0.09 under active contraction. The constant model predicted longer muscle fiber lengths – shifted further to the right on the force-length curve of muscle – which would produce higher passive muscle forces and could lead to unstable conditions in simulations of eccentric contractions.

The most apparent differences across models were observed in reaction force values, with a twelve-fold difference between the constant and linear models (Figure 7C). For the constant model, the reaction force generated by activation was half that of the passive stretch reaction force, while the linear model saw an increase in reaction force from passive stretch to activation, suggesting that increased force transmission efficiency with increasing aponeurosis stiffness does not scale linearly. One variable that we did not investigate with our finite element modeling approach is variability in aponeurosis thickness, which has been shown to affect heterogeneous muscle fiber strain in a finite element model [30]. Future work to couple geometric and material property heterogeneity in muscle-tendon unit modeling would be a benefit to the field and may help to explain the complex behavior of muscle and aponeurosis *in vivo*.

Our muscle slice modeling results also show that the type of function used to model modulus heterogeneity affects aponeurosis strain, muscle fiber strain, and active and passive forces at the muscle-tendon unit level. Despite the fact that both the linear and LNM models were fit to the same set of heterogeneous experimental data (Figure 6B, both fits ~6% normalized root mean square error), these two formulations predicted considerably different aponeurosis fiber and muscle fiber strains, passive stretch reaction force, and active contraction reaction force (Figure 7). Even the LNS model (Figure 6B), which is unlikely to be physiologically accurate, exhibited

less extreme muscle and aponeurosis strains and reaction force values than the linear model (Figure 7). Thus, we recommend against modeling aponeurosis heterogeneity with functions that may yield highly variable aponeurosis properties (such as linear or exponential functions) and recommend the use of functions such as our log normal approach that constrain variability (Figure 2).

Compared to other musculoskeletal tissues, the function of aponeurosis *in vivo* is poorly understood, and recent work has highlighted that aponeurosis does not act in series with muscle [14,17,21,72]. Previous finite element modeling of muscle-tendon units has also shown that muscle mechanics are altered by changes to aponeurosis material properties and geometry [30,32,73,74]. Our results suggest that aponeurosis structure-function heterogeneity can also affect the passive stiffness and force transmission of muscle-tendon units (Figure 7C), and to a lesser extent muscle and aponeurosis strain (Figure 7A-B). Differences in muscle fiber strain that fall within the physiological range (~0.1-0.2 strain, Figure 7B) [4] can manifest in large differences in muscle-tendon stiffness due to the highly nonlinear behavior of passive skeletal muscle [40,75,76]. Thus, researchers should carefully consider the extent to which aponeurosis heterogeneity could impact experimentally observed and simulated muscle-tendon unit behavior.

## **5. Conclusions**

This work aimed to determine the heterogeneous structure function properties of aponeurosis tissue with scanning electron microscopy and materials testing. We found that aponeurosis may exhibit more microstructural collagen waviness in the insertion region (near the tendon) as compared to the transition region (near the muscle midbelly), and a less stiff stress-strain response in the insertion versus transition regions. We also showed that different assumptions of aponeurosis heterogeneity, specifically variations in elastic modulus with location can alter the stiffness and strain of a finite element model of muscle and aponeurosis. Collectively, these results suggest that aponeurosis heterogeneity may be due in part to variations in tissue microstructure and that the associated changes to material properties affect the behavior of computational models of muscle-tendon units.

## **6. Acknowledgements**

Funding for equipment used in this work was provided by the National Science Foundation under Major Research Instrumentation Grant No. 1828082. Authors would like to thank the Bucknell-Geisinger Research Initiative and the Program for Undergraduate Research at Bucknell University for funding to support this work.

## **7. Disclosures**

Mark Seeley is a consultant for Orthopediatrics and receives royalties. Authors have no other disclosures.

## **Citations**

- [1] J. Bojsen-Møller, S.P. Magnusson, Mechanical properties, physiological behavior, and function of aponeurosis and tendon, REVIEW Passive Properties of Muscle J Appl Physiol. 126 (2019) 1800–1807. <https://doi.org/10.1152/jappphysiol.00671.2018>.-During.
- [2] C.M. Eng, T.J. Roberts, Aponeurosis influences the relationship between muscle gearing and force, Journal of Applied Physiology. 125 (2018) 513–519. <https://doi.org/10.1152/jappphysiol.00151.2018>.
- [3] T.J. Roberts, C.M. Eng, D.A. Sleboda, N.C. Holt, E.L. Brainerd, K.K. Stover, R.L. Marsh, E. Azizi, The Multi-Scale, Three-Dimensional Nature of Skeletal Muscle Contraction, Physiology (Bethesda). 34 (2019) 402–408. <https://doi.org/10.1152/physiol.00023.2019>.
- [4] R.L. Lieber, Skeletal Muscle Structure, Function, and Plasticity, Lippincott Williams and Wilkins, Philadelphia, PA, 2010.
- [5] B.J. Raiteri, Aponeurosis behaviour during muscular contraction: A narrative review, European Journal of Sport Science. 18 (2018) 1128–1138. <https://doi.org/10.1080/17461391.2018.1472299>.
- [6] C.J. Zuurbier, P.A. Huijing, Influence of muscle geometry on shortening speed of fibre, aponeurosis and muscle., Journal of Biomechanics. 25 (1992) 1017–1026. [https://doi.org/10.1016/0021-9290\(92\)90037-2](https://doi.org/10.1016/0021-9290(92)90037-2).
- [7] N.M. Fiorentino, F.H. Epstein, S.S. Blemker, ACTIVATION AND APONEUROSIS MORPHOLOGY AFFECT IN VIVO MUSCLE TISSUE STRAINS NEAR THE MYOTENDINOUS JUNCTION, J Biomech. 45 (2012) 647–652. <https://doi.org/10.1016/j.jbiomech.2011.12.015>.
- [8] S.W. Hwang, Y.S. Nam, K. Hwang, S.H. Han, Thickness and tension of the gluteal aponeurosis and the implications for subfascial gluteal augmentation, Journal of Anatomy. 221 (2012) 69–72. <https://doi.org/10.1111/j.1469-7580.2012.01510.x>.
- [9] S.H. Scott, G.E. Loeb, Mechanical properties of aponeurosis and tendon of the cat soleus muscle during whole-muscle isometric contractions, Journal of Morphology. 224 (1995) 73–86. <https://doi.org/10.1002/jmor.1052240109>.
- [10] X. Shan, S. Otsuka, T. Yakura, M. Naito, T. Nakano, Y. Kawakami, Morphological and mechanical properties of the human triceps surae aponeuroses taken from elderly cadavers: Implications for muscle-tendon interactions, PLoS ONE. 14 (2019). <https://doi.org/10.1371/journal.pone.0211485>.
- [11] T. Siebert, A. Tomalka, N. Stutzig, K. Leichsenring, M. Böl, Changes in three-dimensional muscle structure of rabbit gastrocnemius, flexor digitorum longus, and tibialis anterior during growth, J Mech Behav Biomed Mater. 74 (2017) 507–519. <https://doi.org/10.1016/j.jmbbm.2017.07.045>.
- [12] G.J.C. Ettema, P.A. Huijing, Architecture and Elastic Properties of the Series Elastic Element of Muscle-Tendon Complex, in: J.M. Winters, S.L.-Y. Woo (Eds.), Multiple Muscle Systems: Biomechanics and Movement Organization, Springer, New York, NY, 1990: pp. 57–68. [https://doi.org/10.1007/978-1-4613-9030-5\\_4](https://doi.org/10.1007/978-1-4613-9030-5_4).
- [13] A.V. Hill, The Heat of Shortening and the Dynamic Constants of Muscle, Proceedings of the Royal Society B: Biological Sciences. 126 (1938) 136–195. <https://doi.org/10.1098/rspb.1938.0050>.
- [14] F.M. Bossuyt, S. Abramovic, T. Leonard, A. Sawatsky, C.R. Smith, W.R. Taylor, W. Michael Scott, W. Herzog, The non-intuitive, in-vivo behavior of aponeuroses in a

- unipennate muscle, *Journal of Biomechanics*. (2022) 111430.  
<https://doi.org/10.1016/j.jbiomech.2022.111430>.
- [15] M. Epstein, M. Wong, W. Herzog, Should tendon and aponeurosis be considered in series?, *J Biomech*. 39 (2006) 2020–2025. <https://doi.org/10.1016/j.jbiomech.2005.06.011>.
- [16] W. Herzog, The problem with skeletal muscle series elasticity, *BMC Biomed Eng*. 1 (2019) 28. <https://doi.org/10.1186/s42490-019-0031-y>.
- [17] E. Azizi, T.J. Roberts, Biaxial strain and variable stiffness in aponeuroses., *The Journal of Physiology*. 587 (2009) 4309–18. <https://doi.org/10.1113/jphysiol.2009.173690>.
- [18] C.J. Arellano, N.J. Gidmark, N. Konow, E. Azizi, T.J. Roberts, Determinants of aponeurosis shape change during muscle contraction., *Journal of Biomechanics*. (2016). <https://doi.org/10.1016/j.jbiomech.2016.04.022>.
- [19] C.J. Zuurbier, A.J. Everard, P. van der Wees, P.A. Huijting, Length-force characteristics of the aponeurosis in the passive and active muscle condition and in the isolated condition, *J Biomech*. 27 (1994) 445–453. [https://doi.org/10.1016/0021-9290\(94\)90020-5](https://doi.org/10.1016/0021-9290(94)90020-5).
- [20] R.L. Lieber, Can we just forget about pennation angle?, *Journal of Biomechanics*. 132 (2022) 110954. <https://doi.org/10.1016/j.jbiomech.2022.110954>.
- [21] W. Herzog, Skeletal muscle mechanics: Questions, problems and possible solutions, *Journal of NeuroEngineering and Rehabilitation*. 14 (2017). <https://doi.org/10.1186/s12984-017-0310-6>.
- [22] E. Azizi, G.M. Halenda, T.J. Roberts, Mechanical properties of the gastrocnemius aponeurosis in wild turkeys., *Integrative and Comparative Biology*. 49 (2009) 51–8. <https://doi.org/10.1093/icb/icp006>.
- [23] K.L. Grega, R.N. Segall, A.J. Vaidya, C. Fu, B.B. Wheatley, Anisotropic and viscoelastic tensile mechanical properties of aponeurosis: Experimentation, modeling, and tissue microstructure, *Journal of the Mechanical Behavior of Biomedical Materials*. 110 (2020) 103889. <https://doi.org/10.1016/j.jmbbm.2020.103889>.
- [24] X. Shan, S. Otsuka, L. Li, Y. Kawakami, Inhomogeneous and anisotropic mechanical properties of the triceps surae muscles and aponeuroses in vivo during submaximal muscle contraction, *Journal of Biomechanics*. 121 (2021) 110396. <https://doi.org/10.1016/j.jbiomech.2021.110396>.
- [25] X. Miao, T. Shan, J. Wang, The Type and Content of Collagen Fibers of The Levator Aponeurosis In Simple Congenital Blepharoptosis Patients, *Journal of Craniofacial Surgery*. (2019). <https://doi.org/10.1097/scs.00000000000006135>.
- [26] K.S. Miller, B.K. Connizzo, E. Feeney, L.J. Soslowsky, Characterizing local collagen fiber re-alignment and crimp behavior throughout mechanical testing in a mature mouse supraspinatus tendon model, *Journal of Biomechanics*. 45 (2012) 2061–2065. <https://doi.org/10.1016/j.jbiomech.2012.06.006>.
- [27] S.P. Lake, K.S. Miller, D.M. Elliott, L.J. Soslowsky, Effect of fiber distribution and realignment on the nonlinear and inhomogeneous mechanical properties of human supraspinatus tendon under longitudinal tensile loading, *Journal of Orthopaedic Research*. 27 (2009) 1596–1602. <https://doi.org/10.1002/jor.20938>.
- [28] S.P. Lake, K.S. Miller, D.M. Elliott, L.J. Soslowsky, Tensile properties and fiber alignment of human supraspinatus tendon in the transverse direction demonstrate inhomogeneity, nonlinearity, and regional isotropy, *Journal of Biomechanics*. 43 (2010) 727–732. <https://doi.org/10.1016/j.jbiomech.2009.10.017>.

- [29] M. Mohammadkhah, P. Murphy, C.K. Simms, Collagen fibril organization in chicken and porcine skeletal muscle perimysium under applied tension and compression, *Journal of the Mechanical Behavior of Biomedical Materials*. 77 (2018) 734–744. <https://doi.org/10.1016/j.jmbbm.2017.08.007>.
- [30] M.R. Rehorn, S.S. Blemker, The effects of aponeurosis geometry on strain injury susceptibility explored with a 3D muscle model., *Journal of Biomechanics*. 43 (2010) 2574–81. <https://doi.org/10.1016/j.jbiomech.2010.05.011>.
- [31] R.R. Lemos, M. Epstein, W. Herzog, Modeling of skeletal muscle: the influence of tendon and aponeuroses compliance on the force-length relationship., *Medical & Biological Engineering & Computing*. 46 (2008) 23–32. <https://doi.org/10.1007/s11517-007-0259-x>.
- [32] S. Chi, J. Hodgson, J. Chen, V. Reggie Edgerton, D.D. Shin, R.A. Roiz, S. Sinha, Finite element modeling reveals complex strain mechanics in the aponeuroses of contracting skeletal muscle., *Journal of Biomechanics*. 43 (2010) 1243–50. <https://doi.org/10.1016/j.jbiomech.2010.01.005>.
- [33] B.N. Safa, K.D. Meadows, S.E. Szczesny, D.M. Elliott, Exposure to buffer solution alters tendon hydration and mechanics, *Journal of Biomechanics*. 61 (2017) 18–25. <https://doi.org/10.1016/j.jbiomech.2017.06.045>.
- [34] A. Mehdizadeh Kashi, K. Tahemanesh, S. Chaichian, M.T. Joghataei, F. Moradi, S.M. Tavangar, A.S. Mousavi Najafabadi, N. Lotfibakhshaiesh, S. Pour Beyranvand, A. Fazel Anvari-Yazdi, S.M. Abed, How to Prepare Biological Samples and Live Tissues for Scanning Electron Microscopy (SEM), *GMJ*. 3 (2014) 63–80. <https://doi.org/10.31661/gmj.v3i2.267>.
- [35] D.A. Sleboda, K.K. Stover, T.J. Roberts, Diversity of extracellular matrix morphology in vertebrate skeletal muscle, *Journal of Morphology*. 281 (2020) 160–169. <https://doi.org/10.1002/jmor.21088>.
- [36] T. Ushiki, H. Hashizume, S. Itoh, K. Kuboki, S. Saito, K. Tanaka, Low-voltage backscattered electron imaging of non-coated biological samples in a low-vacuum environment using a variable-pressure scanning electron microscope with a YAG-detector, *Journal of Electron Microscopy*. 47 (1998) 351–354. <https://doi.org/10.1093/oxfordjournals.jmicro.a023602>.
- [37] J. Schindelin, I. Arganda-Carreras, E. Frise, V. Kaynig, M. Longair, T. Pietzsch, S. Preibisch, C. Rueden, S. Saalfeld, B. Schmid, J.-Y. Tinevez, D.J. White, V. Hartenstein, K. Eliceiri, P. Tomancak, A. Cardona, Fiji: an open-source platform for biological-image analysis, *Nat Methods*. 9 (2012) 676–682. <https://doi.org/10.1038/nmeth.2019>.
- [38] M. Takaza, K.M. Moerman, J. Gindre, G. Lyons, C.K. Simms, The anisotropic mechanical behaviour of passive skeletal muscle tissue subjected to large tensile strain, *Journal of the Mechanical Behavior of Biomedical Materials*. 17 (2012) 209–220. <https://doi.org/10.1016/j.jmbbm.2012.09.001>.
- [39] B.B. Wheatley, Investigating Passive Muscle Mechanics With Biaxial Stretch, *Front. Physiol*. 11 (2020). <https://doi.org/10.3389/fphys.2020.01021>.
- [40] B.B. Wheatley, G.M. Odegard, K.R. Kaufman, T.L.H. Donahue, How does tissue preparation affect skeletal muscle transverse isotropy?, *Journal of Biomechanics*. 49 (2016) 3056–3060. <https://doi.org/10.1016/j.jbiomech.2016.06.034>.
- [41] S.A. Maas, B.J. Ellis, G.A. Ateshian, J.A. Weiss, FEBio: finite elements for biomechanics., *Journal of Biomechanical Engineering*. 134 (2012) 011005–011005. <https://doi.org/10.1115/1.4005694>.

- [42] D.A. Morrow, T.L. Haut Donahue, G.M. Odegard, K.R. Kaufman, A poroelastic model of skeletal muscle tissue used to predict intramuscular pressure., in: ASME Summer Bioengineering Conference, 2012.
- [43] M. Kauer, V. Vuskovic, J. Dual, G. Szekely, M. Bajka, Inverse finite element characterization of soft tissues, *Medical Image Analysis*. 6 (2002) 275–287. [https://doi.org/10.1016/S1361-8415\(02\)00085-3](https://doi.org/10.1016/S1361-8415(02)00085-3).
- [44] A.J. Vaidya, B.B. Wheatley, An experimental and computational investigation of the effects of volumetric boundary conditions on the compressive mechanics of passive skeletal muscle, *Journal of the Mechanical Behavior of Biomedical Materials*. (2019) 103526–103526. <https://doi.org/10.1016/j.jmbbm.2019.103526>.
- [45] B.B. Wheatley, K.M. Fischenich, K.D. Button, R.C. Haut, T.L. Haut Donahue, An optimized transversely isotropic, hyper-poro-viscoelastic finite element model of the meniscus to evaluate mechanical degradation following traumatic loading, *Journal of Biomechanics*. 48 (2015) 1454–1460. <https://doi.org/10.1016/j.jbiomech.2015.02.028>.
- [46] C.A. Yucesoy, B.H.F.J.M.F.J.M. Koopman, P.A. Huijing, H.J. Grootenboer, Three-dimensional finite element modeling of skeletal muscle using a two-domain approach: linked fiber-matrix mesh model., *Journal of Biomechanics*. 35 (2002) 1253–62. [https://doi.org/10.1016/S0021-9290\(02\)00069-6](https://doi.org/10.1016/S0021-9290(02)00069-6).
- [47] B.B. Wheatley, G.M. Odegard, K.R. Kaufman, T.L. Haut Donahue, Modeling Skeletal Muscle Stress and Intramuscular Pressure: A Whole Muscle Active-Passive Approach., *Journal of Biomechanical Engineering*. 140 (2018) 081006–081006. <https://doi.org/10.1115/1.4040318>.
- [48] R.M. Erskine, D.A. Jones, C.N. Maganaris, H. Degens, In vivo specific tension of the human quadriceps femoris muscle, *European Journal of Applied Physiology*. 106 (2009) 827–838. <https://doi.org/10.1007/s00421-009-1085-7>.
- [49] C.N. Maganaris, V. Baltzopoulos, D. Ball, A.J. Sargeant, In vivo specific tension of human skeletal muscle., *Journal of Applied Physiology (Bethesda, Md. : 1985)*. 90 (2001) 865–72.
- [50] T.D. O'Brien, N.D. Reeves, V. Baltzopoulos, D.A. Jones, C.N. Maganaris, In vivo measurements of muscle specific tension in adults and children., *Experimental Physiology*. 95 (2010) 202–10. <https://doi.org/10.1113/expphysiol.2009.048967>.
- [51] T.C. Pataky, One-dimensional statistical parametric mapping in Python, *Computer Methods in Biomechanics and Biomedical Engineering*. 15 (2012) 295–301. <https://doi.org/10.1080/10255842.2010.527837>.
- [52] O. Beger, M.İ. Karagül, T. Koç, G. Kayan, A. Cengiz, Ş.N. Yılmaz, Z.K. Olgunus, Effects of different cadaver preservation methods on muscles and tendons: a morphometric, biomechanical and histological study, *Anat Sci Int*. 95 (2020) 174–189. <https://doi.org/10.1007/s12565-019-00508-z>.
- [53] S. Jonmarker, A. Valdman, A. Lindberg, M. Hellström, L. Egevad, Tissue shrinkage after fixation with formalin injection of prostatectomy specimens, *Virchows Arch*. 449 (2006) 297–301. <https://doi.org/10.1007/s00428-006-0259-5>.
- [54] M.J. Turunen, H. Khayyeri, M. Guizar-Sicairos, H. Isaksson, Effects of tissue fixation and dehydration on tendon collagen nanostructure, *Journal of Structural Biology*. 199 (2017) 209–215. <https://doi.org/10.1016/j.jsb.2017.07.009>.
- [55] B.B. Wheatley, G.M. Odegard, K.R. Kaufman, T.L. Haut Donahue, A validated model of passive skeletal muscle to predict force and intramuscular pressure, *Biomechanics and*

- Modeling in Mechanobiology. 16 (2017) 1011–1022. <https://doi.org/10.1007/s10237-016-0869-z>.
- [56] S.S. Blemker, P.M. Pinsky, S.L. Delp, A 3D model of muscle reveals the causes of nonuniform strains in the biceps brachii., *Journal of Biomechanics*. 38 (2005) 657–65. <https://doi.org/10.1016/j.jbiomech.2004.04.009>.
- [57] R. Kuravi, K. Leichsenring, M. Böl, A.E. Ehret, 3D finite element models from serial section histology of skeletal muscle tissue – The role of micro-architecture on mechanical behaviour, *Journal of the Mechanical Behavior of Biomedical Materials*. 113 (2021) 104109. <https://doi.org/10.1016/j.jmbbm.2020.104109>.
- [58] L.A. Spyrou, S. Brisard, K. Danas, Multiscale modeling of skeletal muscle tissues based on analytical and numerical homogenization, *Journal of the Mechanical Behavior of Biomedical Materials*. 92 (2019) 97–117. <https://doi.org/10.1016/j.jmbbm.2018.12.030>.
- [59] J.M. Wakeling, S.A. Ross, D.S. Ryan, B. Bolsterlee, R. Konno, S. Domínguez, N. Nigam, The Energy of Muscle Contraction. I. Tissue Force and Deformation During Fixed-End Contractions, *Frontiers in Physiology*. 11 (2020). <https://www.frontiersin.org/articles/10.3389/fphys.2020.00813> (accessed January 3, 2023).
- [60] J.M. Wakeling, M. Jackman, A.I. Namburete, The effect of external compression on the mechanics of muscle contraction., *Journal of Applied Biomechanics*. 29 (2013) 360–4.
- [61] M. Böl, K. Leichsenring, M. Ernst, C. Wick, R. Blickhan, T. Siebert, Novel microstructural findings in M. plantaris and their impact during active and passive loading at the macro level, *Journal of the Mechanical Behavior of Biomedical Materials*. (2015). <https://doi.org/10.1016/j.jmbbm.2015.06.026>.
- [62] M. Böl, K. Leichsenring, C. Weichert, M. Sturmat, P. Schenk, R. Blickhan, T. Siebert, Three-dimensional surface geometries of the rabbit soleus muscle during contraction: input for biomechanical modelling and its validation, *Biomech Model Mechanobiol*. 12 (2013) 1205–1220. <https://doi.org/10.1007/s10237-013-0476-1>.
- [63] J. Kastelic, A. Galeski, E. Baer, The Multicomposite Structure of Tendon, *Connective Tissue Research*. 6 (1978) 11–23. <https://doi.org/10.3109/03008207809152283>.
- [64] L.-H. Yahia, G. Drouin, Collagen structure in human anterior cruciate ligament and patellar tendon, *J Mater Sci*. 23 (1988) 3750–3755. <https://doi.org/10.1007/BF00540523>.
- [65] M. Mohammadkhah, C.K. Simms, P. Murphy, Visualisation of Collagen in fixed skeletal muscle tissue using fluorescently tagged Collagen binding protein CNA35, *Journal of the Mechanical Behavior of Biomedical Materials*. 66 (2017) 37–44. <https://doi.org/10.1016/j.jmbbm.2016.10.022>.
- [66] M. Franchi, M. Fini, M. Quaranta, V. De Pasquale, M. Raspanti, G. Giavaresi, V. Ottani, A. Ruggeri, Crimp morphology in relaxed and stretched rat Achilles tendon, *Journal of Anatomy*. 210 (2007) 1–7. <https://doi.org/10.1111/j.1469-7580.2006.00666.x>.
- [67] S. Stafilidis, K. Karamanidis, G. Morey-Klapsing, G. DeMonte, G.-P. Brüggemann, A. Arampatzis, Strain and elongation of the vastus lateralis aponeurosis and tendon in vivo during maximal isometric contraction, *Eur J Appl Physiol*. 94 (2005) 317–322. <https://doi.org/10.1007/s00421-004-1301-4>.
- [68] E.K. Englund, C.P. Elder, Q. Xu, Z. Ding, B.M. Damon, Combined diffusion and strain tensor MRI reveals a heterogeneous, planar pattern of strain development during isometric muscle contraction., *American Journal of Physiology. Regulatory, Integrative and Comparative Physiology*. 300 (2011) R1079–R1090. <https://doi.org/10.1152/ajpregu.00474.2010>.

- [69] B.J. Raiteri, A.G. Cresswell, G.A. Lichtwark, Three-dimensional geometrical changes of the human tibialis anterior muscle and its central aponeurosis measured with three-dimensional ultrasound during isometric contractions, *PeerJ*. 4 (2016) e2260–e2260. <https://doi.org/10.7717/peerj.2260>.
- [70] B.I. Binder-Markey, D. Sychowski, R.L. Lieber, Systematic review of skeletal muscle passive mechanics experimental methodology, *Journal of Biomechanics*. 129 (2021) 110839. <https://doi.org/10.1016/j.jbiomech.2021.110839>.
- [71] M.L. Palmer, D.R. Clafflin, J.A. Faulkner, A. Panchangam, Non-uniform distribution of strain during stretch of relaxed skeletal muscle fibers from rat soleus muscle, *J Muscle Res Cell Motil*. 32 (2011) 39–48. <https://doi.org/10.1007/s10974-011-9250-0>.
- [72] T. Finni, J.A. Hodgson, A.M. Lai, V.R. Edgerton, S. Sinha, Nonuniform strain of human soleus aponeurosis-tendon complex during submaximal voluntary contractions in vivo, *Journal of Applied Physiology*. 95 (2003) 829–837. <https://doi.org/10.1152/jappphysiol.00775.2002>.
- [73] P. Diniz, C. Quental, P. Violindo, J. Veiga Gomes, H. Pereira, G.M.M.J. Kerkhoffs, F.C. Ferreira, J. Folgado, Design and validation of a finite element model of the aponeurotic and free Achilles tendon, *Journal of Orthopaedic Research*. n/a (2022). <https://doi.org/10.1002/jor.25408>.
- [74] J.A. Hodgson, S.-W. Chi, J.P. Yang, J.-S. Chen, V.R. Edgerton, S. Sinha, Finite element modeling of passive material influence on the deformation and force output of skeletal muscle., *Journal of the Mechanical Behavior of Biomedical Materials*. 9 (2012) 163–83. <https://doi.org/10.1016/j.jmbbm.2012.01.010>.
- [75] S.R. Ward, T.M. Winters, S.M. O’Connor, R.L. Lieber, Non-linear Scaling of Passive Mechanical Properties in Fibers, Bundles, Fascicles and Whole Rabbit Muscles, *Front. Physiol*. 11 (2020). <https://doi.org/10.3389/fphys.2020.00211>.
- [76] B.B. Wheatley, D.A. Morrow, G.M. Odegard, K.R. Kaufman, T.L. Haut Donahue, Skeletal muscle tensile strain dependence: Hyperviscoelastic nonlinearity, *Journal of the Mechanical Behavior of Biomedical Materials*. 53 (2016) 445–454. <https://doi.org/10.1016/j.jmbbm.2015.08.041>.